AIAA 80-1092R

Vortex Shedding as a Source of Acoustic Energy in Segmented Solid Rockets

R. S. Brown,* R. Dunlap,† S. W. Young,‡ and R. C. Waugh‡
United Technologies, Sunnyvale, Calif.

Discrepancies have been observed between the predicted and measured combustion-stability characteristics of the full-scale and subscale Titan segmented solid-propellant rocket motors. Pressure oscillations were generated under conditions which cannot be explained analytically, even allowing for inaccuracies in the propellant parameters. Furthermore, the predicted trend of the acoustic frequency with time is not consistent with the observed trend. This suggests an important source of acoustic energy has been omitted from the analysis. Experimental studies were conducted to examine periodic vortex shedding as an additional source of acoustic energy. These tests were conducted in a cold-flow model of the full-scale Titan SRM. The results demonstrate that periodic flow separations can produce significant pressure oscillations when the shedding frequency approximates the classical acoustic frequency. Hot-wire anemometer data show the magnitude of the regular velocity oscillations, which occur concurrently with the generation of pressure oscillations and exceed the acoustic particle velocity by a factor of 10. Vectorial resolution of the velocity oscillations is consistent with periodically shedding vortices. The data also explain the observed trend of the acoustic frequency with time. The results of this study demonstrate that periodic flow separations can generate significant acoustic energy in solid-propellant rocket motors. Furthermore, this source explains some of the discrepancies between predicted and observed combustion stability behavior in segmented motors.

Introduction

THE spontaneous generation of pressure oscillations in solid-propellant rocket motors has caused significant operational problems in a number of systems. These oscillations, which initially have low amplitude, can couple with the motor case and nozzle to generate substantial acceleration loads on critical system components. Higher amplitudes can result in large changes in the mean pressure which can alter the thrust-time characteristics of the motor and/or cause case failures. Hence, the potential for generating oscillatory pressures must be considered in the design and testing of solid-propellant rocket motors.

The onset of spontaneous oscillatory pressures is determined by a delicate balance between the sources and sinks of oscillatory energy. Acoustic energy is dissipated by dynamic-flow properties of the nozzle (nozzle damping), the oscillatory drag of the condensed-phase combustion products (particle damping), the vibrational characteristics of the grain and case (structural damping), and momentum losses required to accelerate the gases leaving the burning surface to the speed of the chamber gases (flow-turning damping). The response of the propellant-combustion zone to acoustic-pressure and acoustic-velocity oscillations is the primary source of oscillatory energy considered to date. If the sources of acoustic energy exceed the ability of the sinks to dissipate that energy, pressure oscillations grow spontaneously.

Based on these concepts, a combination of analytical[1-3] and experimental methods[4,5] have been developed for estimating the stability of the combustion pressure. These methods have been applied to a wide variety of solid-propellant rocket-motor designs. Comparisons between these predictions and motor test data have shown mixed results.[6,7] Some predictions have agreed with motor data. In other cases, however, low-amplitude pressure oscillations have been generated in a number of motors that were predicted to be stable. Some of these discrepancies resulted from inaccuracies in the propellant-combustion characteristics.[6] In other motors, however, even these inaccuracies were not sufficient to account for the discrepancy between the predicted and observed behavior. Segmented solid-propellant boosters generally fall into this latter category.

Discrepancy between Predictions and Motor Data

Full-Scale Titan Motor

The Titan 304-cm-diam SRM serves as one example where the discrepancy between predicted and observed behavior cannot be resolved by propellant-property inaccuracies. Combustion-stability analyses were conducted on this motor using the Standard Stability Prediction Method for Rocket Motors.[3] The pressure-coupled-response data used in these predictions were obtained from T-burner and rotating-valve data[8] for frequencies between 200 and 900 Hz. For lower frequencies, the response was extrapolated from these data using thermal-wave combustion-response theory. Particle-damping data were obtained from the T-burner tests.[8] No data were available for the velocity response R_v. However, this effect is extremely small compared to the other gains and losses so a response of 1.0 was arbitrarily used. The response to flow turning was assumed to be -1, while the nozzle response was taken as -1.1.

Calculations were made for the first four longitudinal modes at four burn times. The results of these analyses, summarized in Table 1, indicate that these axial modes should be stable, i.e., the predicted net exponential growth rate is negative. Further examination shows that large changes in the contribution from the individual sources and sinks would be required to change the net instability. For example, the particle damping or nozzle loss could be neglected entirely and the motor would still be predicted to be stable at all burn times. The pressure-coupled-response function for propellant would have to be 20 times higher than the experimental value to predict an instability. Since these uncertainties exceed

Presented as Paper 80-1092 at the AIAA/SAE/ASME 16th Joint Propulsion Conference, Hartford, Conn., June 30-July 2, 1980; submitted Aug. 25, 1980; revision received Feb. 23, 1981.

*Senior Staff Scientist, Chemical Systems Division. Associate Fellow AIAA.

†Senior Staff Scientist, Chemical Systems Division. Member AIAA.

‡Research Engineer, Chemical Systems Division.

Table 1 Predicted stability for full-scale Titan motor

Burn depth, cm (burntime, s)	Mode	Frequency, Hz	α_{pc} s^{-1}	α_{vc} s^{-1}	α_{ft} s^{-1}	α_n s^{-1}	α_{pd} s^{-1}	Net α s^{-1}
0	1L	22.20	2.66	0.46	−5.53	−15.78	−2.22	−22
(0 s)	2L	44.51	2.80	0.77	−5.72	−15.5	−4.45	−22
	3L	67.35	2.98	0.92	−5.91	−12.20	−6.74	−21
	4L	90.97	3.32	1.09	−6.10	−11.1	−9.10	−22
20.3	1L	20.31	1.08	−0.17	−4.13	−7.73	−2.03	−14
(22 s)	2L	41.65	1.22	−0.18	−4.14	−7.03	−4.17	−15
	3L	64.18	1.41	−0.14	−4.16	−5.89	−6.42	−16
	4L	87.38	1.65	−0.14	−4.20	−4.60	−8.74	−16
44.5	1L	21.81	0.60	−0.22	−3.43	−5.07	−2.18	−17
(47 s)	2L	44.14	0.75	−0.24	−3.34	−4.70	−4.41	−12
	3L	67.55	0.93	−0.22	−3.38	−4.08	−6.76	−14
	4L	91.58	1.14	−0.17	−3.36	−3.39	−9.16	−15
69.9	1L	23.74	0.44	−0.18	−2.43	−3.88	−2.37	−9
(77 s)	2L	47.56	0.53	−0.14	−2.31	−3.81	−4.76	−11
	3L	71.47	0.65	−0.13	−2.25	−3.60	−7.15	−13
	4L	96.20	0.81	−0.10	−2.26	−3.41	−9.62	−15

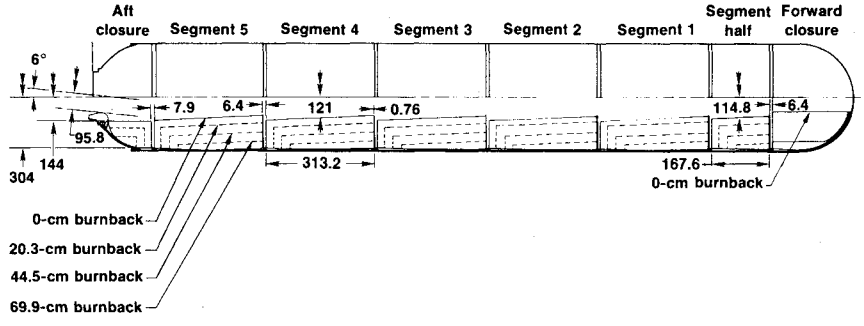

Fig. 1 Schematic diagram of Titan 34D.

reasonable error limits, one would conclude that the motor should not spontaneously generate pressure oscillations at any time during the firing.

Unfortunately, this is not the case. Data from early test firings of the Titan suggested that low-amplitude pressure oscillations might be present.[9] Fortunately, the oscillations did not compromise the operational characteristics of this motor. Because of the recent concern with pressure oscillations in the Shuttle SRB,[10] high-frequency-response, high-resolution pressure transducers were added to recent full-scale tests of the Titan to monitor the chamber-pressure oscillations. One transducer (PK1) monitored the chamber pressure in the igniter while a second transducer (PK2) monitored the chamber pressure at the head end of the motor directly. The frequency response of the attachment tubing was tested and found to be faithful to 250 Hz. Between 250 and 1000 Hz, the frequency components could still be detected but amplitude errors of +50% were possible.[7] Additionally, high-response solid-state strain gages were mounted at the axial midpoint of each segment, including the short head-end segment, to monitor the oscillatory hoop strain. Figure 1 shows a schematic diagram of the motor and the internal geometry at various web burnbacks.

Frequency spectral analyses of the high-response pressure data and strain data were conducted to determine the magnitude of the frequency components in the oscillatory pressure and case strains. Figure 2 shows a plot obtained by AFRPL of the pressure amplitude/frequency spectra as a function of burntime measured by PK2 during the first test. The calculated acoustic frequency of the first four longitudinal modes is also shown as a function of burntime. Excitation of the first (23 Hz) and the second (47 Hz) longitudinal modes is clearly evident. Figure 3, which shows the corresponding data from the second full-scale motor test, demonstrates the repeatability of the results. Figure 4 shows the frequency spectra of the hoop strain at the aft end of the motor obtained from the first test. Data from the second test duplicate these results. Again, the presence of the first acoustic mode is obvious throughout most of the firing. There is also some evidence of oscillations at the second longitudinal mode. In no case, however, did the oscillations in either motor compromise the ballistic performance in any way.

A number of observations can be made from these data. First, the data contradict the stability predictions shown in Table 1. Second, the predictions show the fundamental mode should be the most stable (since α_{net}/f has the largest magnitude), while the higher modes decrease in stability with increasing mode number. However, the data show the fundamental modes to be the least stable and the higher modes to be more stable. Third, the observed trend of frequency with time does not follow the acoustic predictions between 30 and 55 s in all three waterfall plots. The data show the characteristic frequencies decrease with time while the predicted frequencies increase with time. An explanation for this behavior will be offered later in the paper. At this point, it is sufficient to note that the classical acoustic frequencies may not provide accurate predictions for the characteristic frequencies.

Subscale Titan Motor

The subscale Titan motors provide another example of the discrepancy between stability predictions and motor data. These motors, which were 1/6.55 scaled versions of the full-

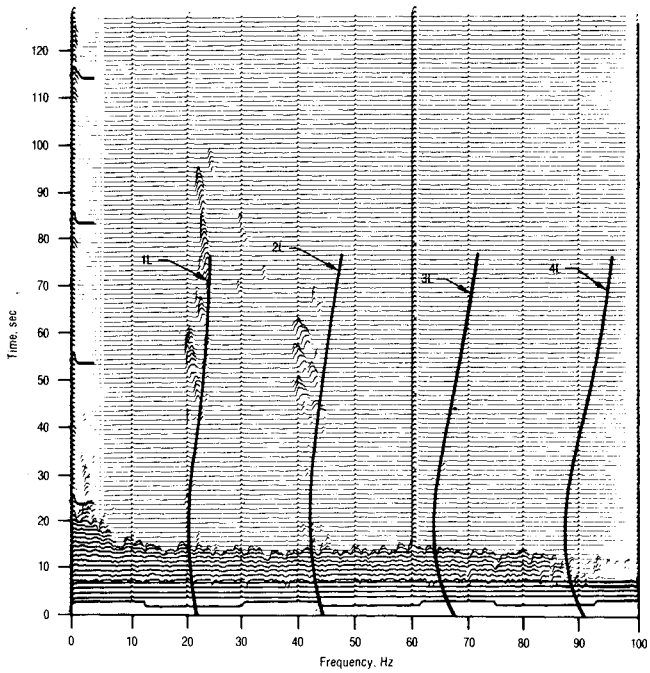

Fig. 2 Waterfall of Kistler data from Titan 34D.

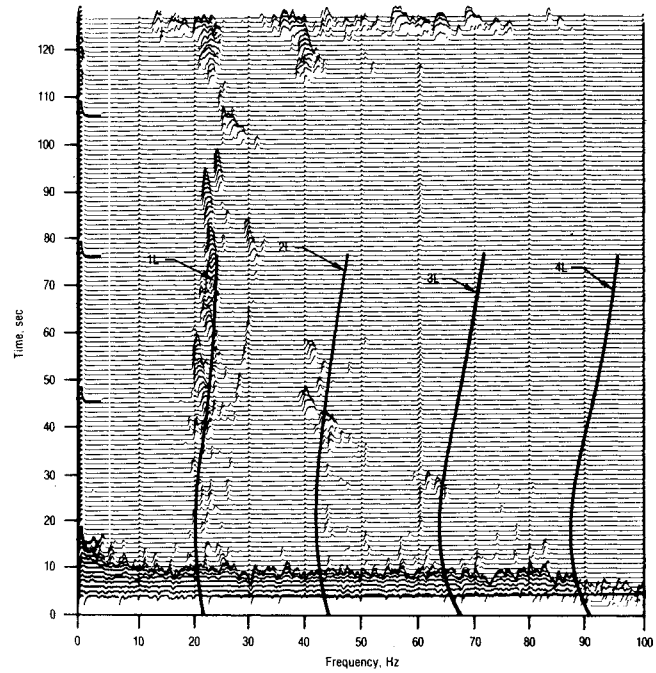

Fig. 4 Waterfall of hoop strain on aft segment.

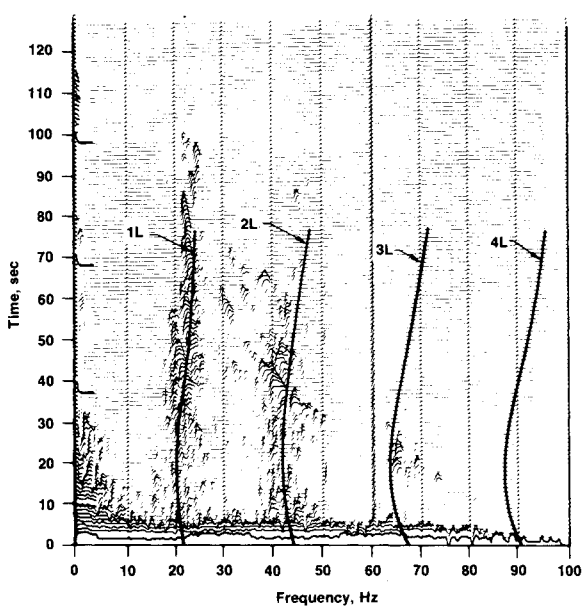

Fig. 3 Waterfall of Kistler data from Titan 34D.

scale motor, were also fired as part of a recent test program. Stability predictions were also made for these motors using the Standard Stability Prediction Method.[3] The results of these calculations, presented in Table 2, again show that the first four longitudinal modes should be stable in this motor as well. As in the full-scale motor, the largest sources of damping could contain large errors without influencing the net stability predictions.

The oscillatory chamber pressure at the head end of the motor was monitored with two high-frequency pressure transducers during two tests. Radially responding accelerometers were also located on each segment at the midpoint between the end flanges. Spectral analyses were made on each of the pressure transducers at four time intervals during each test. The results from the first test are shown in Figs. 5-7. (The data from the second test duplicated these results.) These spectra show this motor generates broadband-frequency spectrum shortly after ignition. At approximately 6 s into the test (which corresponds to 36 s of burning in the full-scale Titan motor), pressure oscillations having an amplitude of approximately 2% of the mean pressure were observed. Peaks in the frequency spectra appear at 120 and 250 Hz, which closely correspond to the predicted first and second classical acoustic axial modes of the motor. These modes were also present at 7 and 9 s, while at 12 and 14 s they became less organized.

The corresponding accelerometer data showed no particular response at these frequencies. In fact, all the vibrational energy appears to have occurred at frequencies above 400 Hz. Hence, the accelerometers did not provide a good indication of the internal-acoustic-pressure environment in the motor. Since the cases had thick steel walls and had heavy flanges at each end, they were very stiff and would not necessarily transmit the low-frequency pressure oscillations.

Again, there is a large discrepancy between the predicted and observed stability behavior in this motor. The fundamental mode, predicted to be the most stable, oscillates through much of the firing. Additionally, the second longitudinal mode, predicted to be the second-most stable mode, is also excited throughout much of the firing. Hence, the subscale motor provides behavior which is consistent with the full-scale motor but contradicts the predicted behavior.

Additional Evidence

In addition to the Titan motors, the same discrepancy is found when predictions and data for the Space Shuttle Booster (SRB) are compared. Mathes[10] predicted this motor would be stable over a wide range of motor geometries and propellant properties. However, low-amplitude pressure oscillations and, hence, thrust oscillations have been observed in several firings of this motor. ONERA also appears to have experienced low-amplitude pressure oscillations in one of their large solid-propellant motors.[11] They also were unable to reconcile the generation of pressure oscillations to conventional stability analyses.

Vortex Shedding as an Acoustic Energy Source

The preceding discussion documented two examples that have significant differences between observed and predicted combustion-stability behavior. In addition, two other

Table 2 Predicted stability for subscale Titan motor

Burn depth, cm	Mode	Frequency, Hz	α_{pc} s^{-1}	α_{vc} s^{-1}	α_{ft} s^{-1}	α_n s^{-1}	α_{pd} s^{-1}	Net α s^{-1}
0	1L	118.06	17.7	−2.60	−38.59	−103.0	−11.81	−135
	2L	264.06	36.1	−1.87	−40.73	−101.0	−26.41	−142
	3L	423.71	55.6	−0.69	−41.24	−103.0	−42.37	−130
	4L	586.56	80.5	0.21	−42.23	−86.0	−58.66	−106
3.10	1L	121.91	9.01	−3.42	−26.45	−52.0	−12.19	−82
	2L	263.75	18.8	−2.69	−26.09	−53.0	−26.38	−87
	3L	414.56	27.8	−1.95	−25.67	−45.0	−41.46	−84
	4L	566.41	37.0	−1.09	−24.48	−43.0	−56.64	−77
6.78	1L	132.47	5.89	−2.79	−20.11	−33.3	−13.25	−61
	2L	273.85	12.2	−2.92	−19.04	−32.3	−27.39	−66
	3L	423.25	18.9	−1.89	−18.24	−28.0	−42.32	−70
	4L	572.13	24.6	−0.81	−17.02	−21.0	−57.21	−71
10.67	1L	147.50	4.51	−1.66	−14.82	−23.61	−14.75	−60
	2L	295.37	8.45	−2.17	−13.42	−22.53	−29.54	−59
	3L	444.45	12.9	−1.34	−12.40			
					0	−21.43	−44.45	−67
	4L	591.76	16.8	−0.19	−12.01	−19.19	−59.18	−75

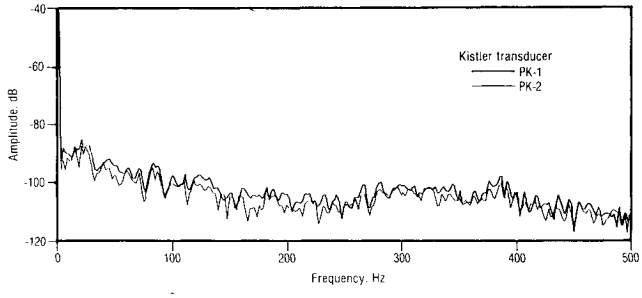

Fig. 5 Titan 34D subscale test 3; time −0.5 to 2.5 s.

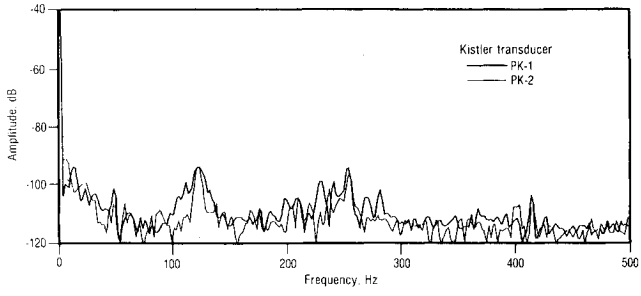

Fig. 6 Titan 34D subscale test 3; time −6 to 9 s.

examples have been cited which also fit this pattern. This suggests there is an important source of acoustic energy in each of these motors which was not considered in the stability predictions. Each is a large-segmented (or pseudosegmented, in the case of ONERA) solid-propellant motor. Thus, the missing acoustic-energy source appears to be related to some characteristic of this type of motor.

Flandro and Jacobs[12] first suggested that unstable flow separations in solid-propellant rocket motors could couple with the chamber acoustics to provide an additional source of acoustic energy. The fact that periodic flow oscillations can be significant sources of acoustic energy has been known for some time. Lord Rayleigh[13] studied the acoustics of bird calls nearly 100 yr ago; numerous studies have been conducted on this subject since. Figure 8 shows demonstrated examples where unstable separated flows can couple with the acoustics to produce a significant source of acoustic energy. These geometries show a number of similarities with the internal

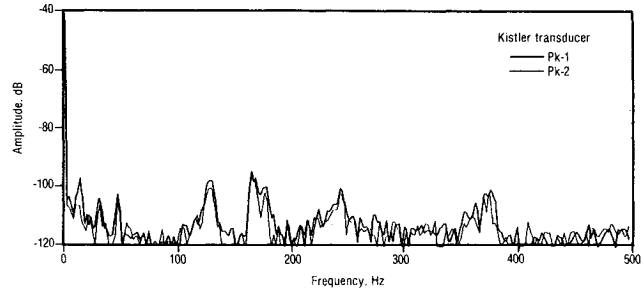

Fig. 7 Titan 34D subscale test 3; time −12 to 14 s.

configuration of segmented solid-propellant rocket motors, shown in Fig. 9.

This hypothesis is also supported by the recent experimental results of Culick and Magiawala[14] and Dunlap and Brown.[15] Both experiments were conducted in flow geometries that simulate gas flow over multiple protruding restrictors. Both studies showed significant acoustic-energy generation when the shedding frequency equals one of the acoustic frequencies. Furthermore, both studies showed the strength of the source depends on the gas velocity through the restrictors and the restrictor separation.

This additional source of acoustic energy also provides a qualitative explanation for the frequency-time data obtained during the full-scale Titan tests. The effect of the flow velocity on the frequency of the unstable flow separation (i.e., vortex shedding) is characterized by critical values of the Strouhal number, $f_S l/U$. Chanaud and Powell[16] showed that these critical Strouhal numbers could be relatively close together (i.e., 0.42 vs 0.56). Referring to Fig. 2, note that pressure oscillations appear at approximately 45 s into the firing. As the motor burns, the restrictor diameter increases and the linear gas velocity decreases. At constant Strouhal number, this leads to a decreasing shedding frequency. Eventually, there is enough discrepancy between the shedding frequency and the acoustic frequency to significantly reduce the generation of acoustic energy. This would explain the damping of the oscillations at 62 s. At 64 s, however, the conditions at the next-higher critical Strouhal number begin to correspond to the acoustic-mode frequency and the oscillations reappear. Thus, both the growth and decay of the oscillations and the trend of frequency with time are consistent with the hypothesis that periodically shedding vortices are providing the additional acoustic energy.

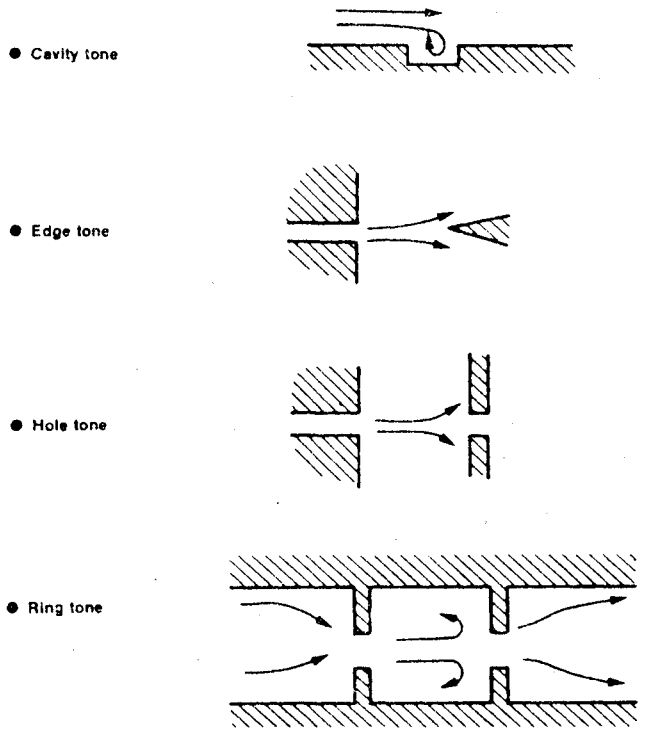

Fig. 8 Examples of sound generation by flow separations.

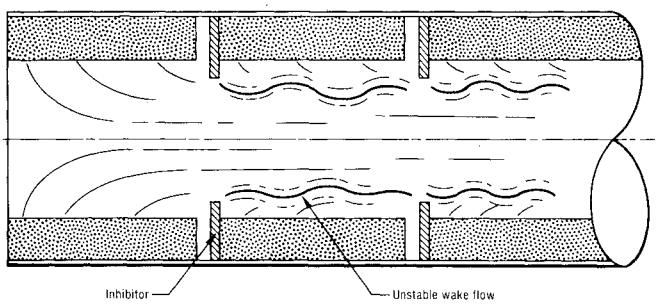

Fig. 9 Generation of unstable wake flow.

Verification in a Cold-Flow-Model Rocket

Based on these observations, CSD conducted a series of tests to evaluate the role of periodic vortex shedding in the acoustic driving of solid-propellant rocket motors. In another program, CSD conducted a detailed study of the simulated internal flowfield in the Titan using subscale cold-flow simulation models. These cold-flow models provided exact geometry and Mach-number scaling of the full-scale motors. The Reynolds number was also scaled within a factor of 6 (Ref. 17). Since the Reynolds number is of the order of 2×10^7 in the full-scale motor, exact Reynolds-number scaling is not required. Hence, these models provided an excellent facility in which to investigate vortex shedding as an acoustic-energy source.

Apparatus and Instrumentation

The cold-flow models of the Titan were scaled to 4.65% of the full-scale motor and had an internal grain diameter of 14 cm. The burning-propellant surfaces were simulated by nitrogen flowing through tapered porous bronze filters. Interchangeable 0.08-cm-thick plates simulated the restrictors on the forward side of each segment. These restrictors are used to control the ballistics of the full-scale motor. The diameter of these restrictors relative to the grain diameter was estimated to be 0.71 for segment 1, 0.68 for segment 2, 0.76 for segment 3, 0.98 for segment 4, and 1.00 for segment 5. Spacer tubes were used to simulate the slots between the segments. These spacers also provided access for anemometers and pressure transducers. Additional details on the equipment are presented in Ref. 7.

Hot-wire anemometers, split-film probes, and Kistler pressure transducers were used to monitor the oscillatory-flow environment. Mean-pressure measurements were made using strain-gage transducers. All the tests were run at a 275-kPa chamber pressure.

Table 3 Acoustic-mode frequencies

Mode	Frequency, Hz
First axial	183
Second axial	365
Third axial	550
Fourth axial	738

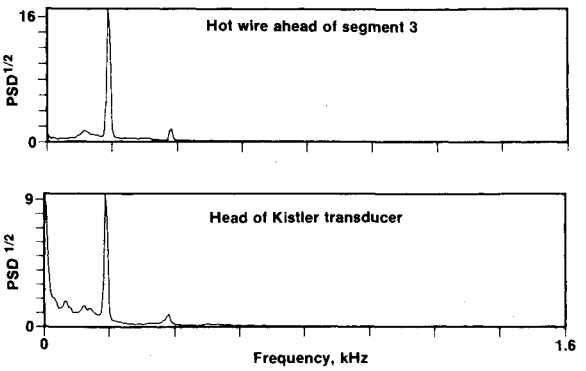

Fig. 10 Response of 69.9-cm model.

Table 4 Flow conditions at resonance in 69.9-cm model

Slot	Mach No. at C/L	Strouhal No. (based on diameter)	Strouhal No. (based on length)
2	0.040	1.07	2.04
3	0.076	0.63	1.08
4	0.096	0.64	0.85
5	0.112	0.56	0.73

Acoustic-Mode Calculation

Predictions of the acoustic-mode frequencies were made for the 69.9-cm model using a NASTRAN finite-element model. This geometry was selected for detailed testing because organized spontaneous velocity oscillations were observed during the mean-flow-profile studies.[17] The calculations were based on nitrogen at 275 kPa and 4.5°C, giving a sound speed of 340 m/s. The results of the calculations are summarized in Table 3. The predicted acoustic-pressure distributions closely follow a cosine mode shape for each of the modes. It should be noted that the NASTRAN approach assumes all of the cavity walls are rigid and the cavity gases have no mean flow. Hence, the calculations do not consider the effects of wall damping (or driving) and mean flow on the acoustic frequencies and their associated acoustic-pressure and velocity distributions. Therefore, the actual resonant frequencies can differ slightly from the calculated values.

Cold-Flow-Model Test Results

In the mean-flow studies in the 69.9-cm burnback model, large-amplitude velocity oscillations were measured by the centerline anemometer just upstream of the third restrictor.[17]

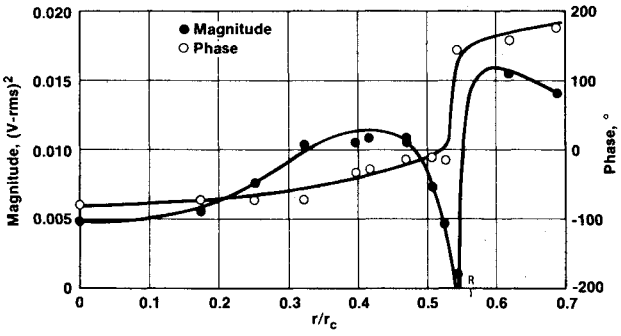

Fig. 11 Cross power at 188 Hz near center of segment two.

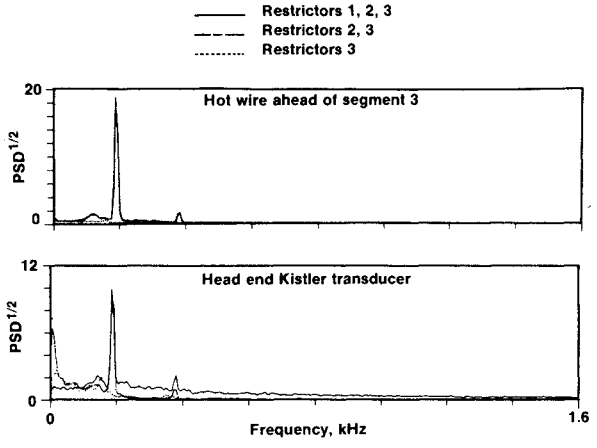

Fig. 12 Effect of restrictor combination in 69.9-cm model.

Since the full-scale Titan motor also generated oscillations at this burnback, the cold-flow tests were repeated in this study to measure the frequency spectra of both the anemometer and the head-end transducer. Figure 10 shows the spectrum of the hot-wire output on the upper plot while the spectrum of the head-end pressure is shown on the lower plot. The dominant frequency in both plots occurs at 188 Hz, which corresponds closely to the fundamental mode of 183 Hz. Strouhal numbers based on restrictor diameter and on restrictor spacing were calculated for the mean flow through each of the restrictors. These numbers, shown in Table 4, are all in the range where periodic vortex shedding would be expected. In addition, these spectra also show that low-amplitude velocity and pressure oscillations were generated at the second acoustic frequency. This is consistent with the observation of multiple critical Strouhal numbers in other geometries.

At first, one might expect that the anemometer was responding to the acoustic-particle velocity associated with the pressure wave. Quantitative analysis of the data, however, reveals that this is not the case. The normalized pressure amplitude at the head end was 0.065% of the mean pressure and, hence, the amplitude of the acoustic-particle Mach number at the third segment would be approximately 0.00065. The anemometer measurements, however, showed the oscillatory Mach number to be 0.006, nearly an order of magnitude higher. This suggests relatively large-magnitude flow instabilities were generating the oscillatory pressures. Furthermore, this would indicate the velocity oscillations were relatively inefficient in generating pressure oscillations for this particular set of conditions.

The axial distribution of the velocity oscillations was explored to determine if they were consistent with periodic vortical flows. In one set of experiments, two hot-wire anemometers were located at the axial midpoint of the second segment. One hot wire was held stationary at the radial location of the maximum fluctuating-voltage measurement

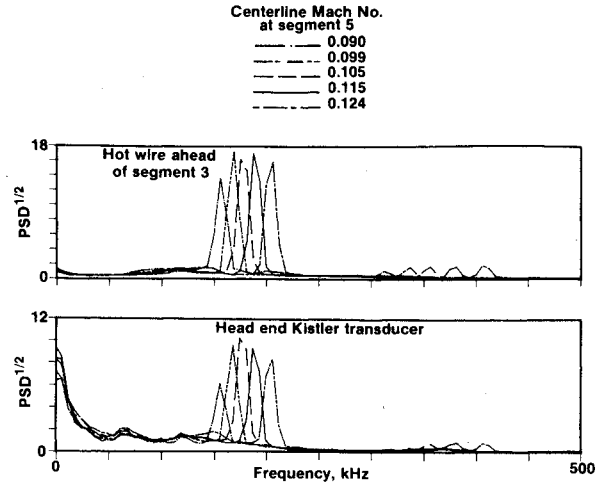

Fig. 13 Effect of Mach number in 69.9-cm model.

(i.e., the high-speed region of the vortex) and the other wire was traversed radially. The cross power at 188 Hz was then measured as the traversing wire was moved across the radius.

If periodically shedding vortices were being generated, one would expect the magnitude of the cross power to be relatively high when both wires were in the high-speed regions of the vortex flow. Furthermore, there should be a relatively low phase angle between the output of the two anemometers if both wires are on the same side of the vortex. With the traversing wire in the core of the vortex, the cross power should drop significantly and the phase angle should increase significantly. With the traversing wire on the opposite side of the vortex from the fixed wire, the magnitude of the cross power should increase and the phase angle should approach 180 deg.

Figure 11 shows the magnitude and phase of the cross-power spectra as a function of radial position. Note the data follow the expected magnitude and phase relationships. Furthermore, the minimum in the magnitude of the oscillations and the phase change occur near the radial position of the upstream restrictor (R in Fig. 11). Thus, the radial distribution of the cross power is consistent with periodic shedding of vortices at 188 Hz. Other data[7] provide additional support for this conclusion.

Studies were then conducted to determine which combination of restrictors produced this coupling. Tests were run with restrictors: 1) on the upstream face of the three forward segments, 2) on the upstream face of the second and third segments, and 3) on the third segment only. Since the restrictors in front of the fourth and fifth segments were essentially flush with the propellant surface, they were not considered in these tests. Figure 12 shows the spectra from the anemometer upstream of the third segment and the corresponding spectra from the head-end Kistler transducer. These data show the restrictors on the second and third segments are the acoustically active pair producing the pressure oscillations. This restrictor pair is located near the velocity antinode which is consistent with the laboratory data reported by Dunlap and Brown.[15]

Tests were conducted in which the Mach number of gas flow was varied by maintaining a constant chamber pressure and changing the nozzle area with a pintle assembly. The spectra from the hot wire located upstream of the third segment and the spectra from a head-end pressure transducer data are compared in Fig. 13 as a function of chamber Mach number. Again, the upper plot is the power-spectral density of the oscillatory velocity and the lower plot is the power-spectral density of the oscillatory pressure.

The number of interesting observations can be made from these data. First, the dominant frequency in both velocity and pressure oscillations depends on mean-flow speed of the gases

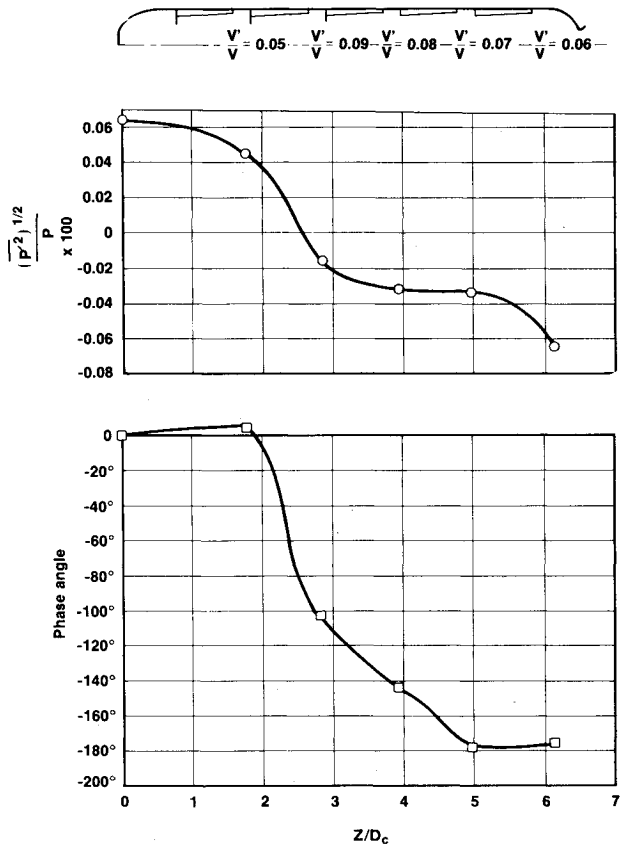

Fig. 14 Acoustic-pressure and velocity data in 69.9-cm model.

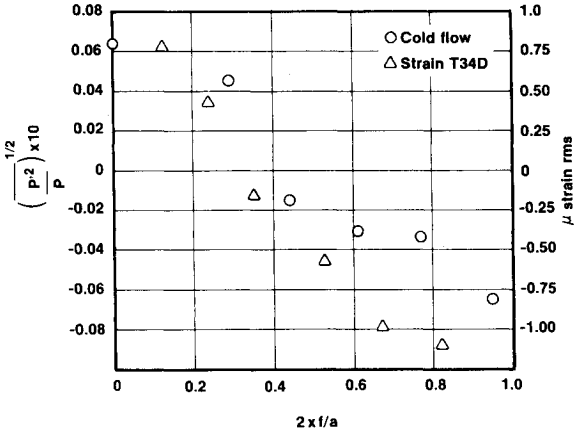

Fig. 15 Mode-shape comparison.

in the chamber and is not determined by the classical acoustic modes of the cavity. Second, the frequency decreases as the flow speed decreases. Since the ratio of frequency to Mach number is nearly constant, a constant Strouhal number appears to be the proper correlating parameter. Third, the amplitude of the pressure oscillations is a maximum when the frequency matches the classical acoustic mode of the cavity. This behavior is characteristic of the response of a driven damped oscillator. Fourth, the amplitude of the velocity and pressure oscillations also depend on the proximity of the dominant frequency to the acoustic frequency. The effect on the velocity amplitude, however, is not as strong as the effect on the pressure amplitude. This suggests the possibility of feedback from the pressure oscillation to the velocity oscillation.

Measurements were also made to determine the axial variation of the pressure oscillations. Kistler pressure transducers were mounted on each of the spacer sections between the segments along the longitudinal axis. The pressure amplitude and the phase angle referenced to the head-end transducer were measured at each of these locations. These data, shown in Fig. 14, are characteristic of a damped axial mode. It should be noted that significant acoustic damping would be expected from the porous walls and from the nozzle; hence, one would expect this damping to be reflected in the mode shape. It is interesting to note that the pressure node appears to have shifted toward the source of vortex shedding.

Comparisons between Model and Motor Data

The data from these cold-flow experiments were also compared to the full-scale motor data. If one assumes that oscillatory vibrations in the case were generated by local pressure distributions (i.e., there is no transmission of oscillatory strain down the length of the motor), then the strain oscillatory data should reflect the modal distribution of acoustic pressure. Hence, in this analysis, the oscillatory hoop strain data from the full-scale motor were compared to the acoustic-pressure-distribution data from the model. This comparison, shown in Fig. 15, shows good agreement between the model and the motor. The abscissa, $2f/a$, accounts for the substantial differences in the sound speed and the motor length. The agreement is remarkably good considering the large size and temperature differences. Note that the data suggest the pressure node was shifted towards the head end in both the cold-flow model and the full-scale motor.

Conclusions

The results of these studies have demonstrated that periodic shedding of vortices can provide a significant source of acoustic energy in segmented solid-propellant motors. Cold-flow tests have demonstrated the generation of acoustic-pressure oscillations near the fundamental mode. Anemometer measurements of the oscillatory flow establish that periodic vortical-flow patterns are generated simultaneously with the pressure oscillations. The change in velocity magnitude and phase characteristics with radial position are consistent with vortical flows. Two restrictors located at the velocity antinode provide the critical geometry. In addition, the characteristic frequency varies with the mean chamber speed as expected for flow-driven sound generation.

Key characteristics of the model data agree with the motor results. The characteristic frequencies and mode shapes indicate excitation of the fundamental longitudinal mode in both cases. The change in characteristic frequency with time (i.e., flow speed) is consistent with vortex shedding in both the model and the full-scale motor. Thus, the composite results of this study provide a qualitative explanation for the discrepancy between the predicted stability characteristics and the motor data.

Acknowledgments

The authors wish to express their sincere thanks to D.R. Luther, W.A. Langley, and T. Park of AFRPL for providing the waterfall plots, to P.G. Willoughby who designed the cold-flow model, and to G.A. Flandro, L.K. Isaacson, F.E.C. Culick, and R.A. Beddini for many helpful and stimulating technical discussions.

This study was conducted under Air Force Contract F04701-77-C0060 with funding and technical direction provided by the Air Force Rocket Propulsion Laboratory.

References

[1] Culick, F.E.C., "Stability of Three-Dimensional Motions in a Combustion Chamber," *Combustion Science and Technology*, Vol. 10, 1975, pp. 109-124.

[2] Cantrell, R.H. and Hart, R., "Interaction Between Sound and Flow in Acoustic Cavities: Mass, Momentum, and Energy Considerations," *Journal of the Acoustical Society of America*, Vol. 36, April 1964, pp. 697-706.

[3] Lovine, R.L. and Waugh, R.C., "Standard Stability Prediction Method for Solid Rocket Motors," CPIA Publication 273, Aug. 1975.

[4] Kraeutle, K.J., "Particle Size Analysis in Solid Propellant Research," *Experimental Diagnostics in Combustion of Solids, Progress in Astronautics and Aeronautics,* Vol. 63, edited by T.L. Boggs and B.T. Zinn, AIAA, New York, 1978, pp. 76-108.

[5] Brown, R.S., Culick, F.E.C., and Zinn, B.T., "Experimental Methods for Combustion Admittance Measurements," *AIAA Progress in Astronautics and Aeronautics Experimental Diagnostics in Combustion of Solids,* Vol. 63, edited by T.L. Boggs and B.T Zinn, AIAA, New York, 1978, pp. 191-220.

[6] Beckstead, M.W., Krashin, M., Butcher, A.G., Pilcher, D.L., "Acoustic Stability Characterizations of the Trident I (C4) Motors," *11th JANNAF Combustion Meeting,* CPIA Publication 261, Dec. 1974, pp. 535-565.

[7] Brown, R.S. et al., "Vortex Shedding Studies," AFRPL TR-80-13, Air Force Rocket Propulsion Laboratory, Edwards AFB, Calif., April 1980.

[8] Brown, R.S., Erickson, J.E., and Babcock, W.R., "Combustion Response Function Measurement by the Rotating Valve Method," *AIAA Journal,* Vol. 12, No. 11, 1974, pp. 1502-1510.

[9] Purdy, R.W., "Static Motor Analog Chamber Pressure Analysis," Titan III/M Crew Safety Studies, Report UTC-480268-48, Feb. 1968.

[10] Mathes, H.B., "Assessment of Chamber Pressure Oscillations in Shuttle Solid Rocket Booster Motor," AIAA Paper 80-1091 presented at 16th Joint Propulsion Conference, Hartford, Conn., June 1980.

[11] Kuntzmann, P., "Etudes Recentes a L'ONERA Sur Les Instabilities De Combustion Dans Les Moteurs Fusecs a Propergol Solid," AGARD-CP-259, April 1979, pp. 22-1-22-24.

[12] Flandro, G.A. and Jacobs, H.R., "Vortex-Generated Sound in Cavities," *AEROACOUSTICS: Jet and Combustion Noise; Duct Acoustics, Progress in Astronautics and Aeronautics,* Vol. 37, edited by H.T. Nagamatsu, AIAA New York, 1973, pp. 521-533.

[13] Lord Rayleigh, *Theory of Sound,* Vol. 2, Dover Publications, 1945, pp. 410-412.

[14] Culick, F.E.C. and Magiawala, K., "Excitation of Acoustic Modes in a Chamber by Vortex Shedding," *Journal of Vibration and Sound,* Vol. 64, No. 3, 1979, pp. 455-457.

[15] Dunlap, R. and Brown, R.S., "Preliminary Experiments on Acoustic Oscillations Driven by Periodic Vortex Shedding," submitted to *Journal of Spacecraft and Rockets,* April 1980.

[16] Chanaud, R.C. and Powell, A., "Some Experiments Concerning the Hole and Ring Tone," *Journal of the Acoustical Society of America,* Vol. 37, May 1965, pp. 902-911.

[17] Dunlap, R., Willoughby, P.L., and Young, S.W., "Cold-Flow Studies Test Report," Test Report CSD 4901-79-135, Chemical Systems Division/UTC, March 1980.